

Schrödinger’s Navigator: Imagining an Ensemble of Futures for Zero-Shot Object Navigation

Yu He^{1,4}, Da Huang^{2,4}, Zhenyang Liu^{1,4}, Zixiao Gu¹, Qiang Sun³

Guangnan Ye^{1,4,†}, Yanwei Fu^{1,4,†}, Yu-Gang Jiang¹

¹Fudan University ²Shanghai Jiao Tong University

³Shanghai University of International Business and Economics ⁴Shanghai Innovation Institute

Project Page: <https://heyu322.github.io/Schrodinger-Navigator.github.io/>

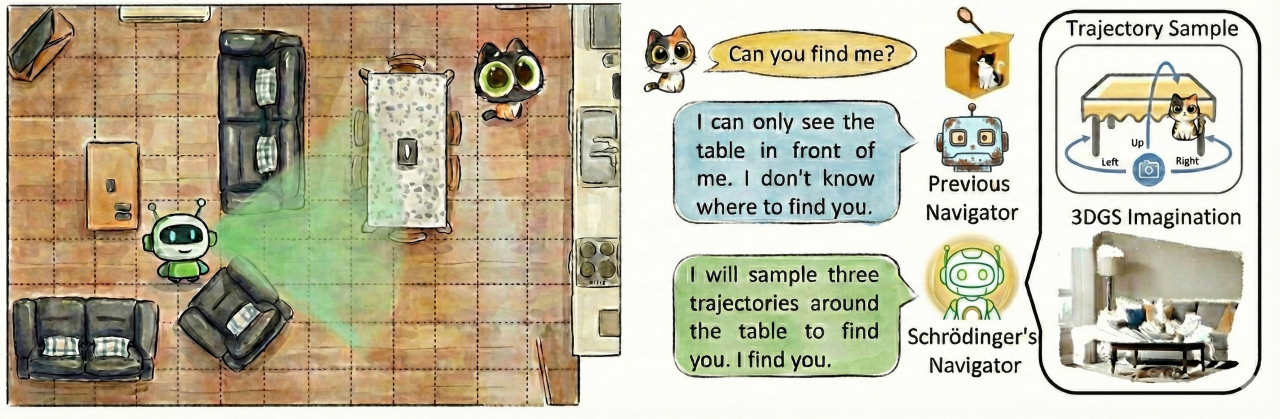


Fig. 1: Real-world zero-shot object navigation often fails when the target object (e.g., a cat) is hidden behind occlusions and surrounded by unknown or potentially hazardous space. Conventional navigation systems typically perceive only the immediate occluder and are unable to infer what exists beyond it. Our Schrödinger’s Navigator addresses this challenge by modeling the unobserved regions as multiple plausible futures.

Abstract—Zero-shot object navigation (ZSON) requires robots to locate target objects in unseen environments without task-specific fine-tuning or pre-built maps, a capability crucial for service and household robotics. Existing methods perform well in simulation but struggle in realistic, cluttered environments where heavy occlusions and latent hazards make large portions of the scene unobserved. These approaches typically act on a single inferred scene, making them prone to overcommitment and unsafe behavior under uncertainty. To address these challenges, we propose Schrödinger’s Navigator, a belief-aware framework that explicitly reasons over multiple *trajectory-conditioned imagined 3D futures* at inference time. A trajectory-conditioned 3D world model generates hypothetical observations along candidate paths, maintaining a superposition of plausible scene realizations. An adaptive, occluder-aware trajectory sampling strategy focuses imagination on uncertain regions, while a *Future-Aware Value Map* (FAVM) aggregates imagined futures to guide robust, proactive action selection. Evaluations in simulation and on a physical Go2 quadruped robot demonstrate that Schrödinger’s Navigator outperforms strong ZSON baselines, achieving more robust self-localization, object localization, and safe navigation under severe occlusions and latent hazards. These results highlight the effectiveness of reasoning over imagined 3D futures as a scalable and generalizable strategy for zero-shot navigation in uncertain real-world environments.

I. INTRODUCTION

Object navigation is a core capability for mobile robots operating in real-world environments [7, 1, 5]. For practical deployment in service robotics and household assistance, an agent must efficiently search for target objects in previously unseen environments—without access to *pre-built maps* [6, 9, 21] or costly task-specific retraining for each new scene [53, 35]. Zero-shot object navigation (ZSON) captures this challenge by requiring a robot to locate a specified object in a novel environment without any task-specific fine-tuning [26, 12], thereby emphasizing the need for transferable semantic understanding and robust priors that generalize across environments.

Although recent ZSON methods have demonstrated promising performance in simulation and simplified settings, their effectiveness often degrades in realistic, cluttered environments, where robots must contend with heavy occlusions and previously unseen risks [50, 12, 45, 39, 4]. In such scenarios, a robot’s perception of the world is inherently partial and uncertain: *substantial portions of the scene remain unobserved behind obstacles*, as illustrated in Figure 1, where the target cat is occluded by the table. Moreover, both targets and hazards may appear or disappear as the robot moves and its viewpoint

[†] Corresponding authors.

changes.

Existing ZSON approaches struggle under these conditions. They frequently fail when target objects are hidden behind severe static occlusions or when environments contain unknown risks that are not directly observable. These failures expose a fundamental limitation: current methods typically act on a single inferred scene interpretation, without explicitly reasoning over multiple plausible configurations of the unobserved space before taking action. As a result, they are prone to overcommitting to local observations and become easily misled in cluttered, occlusion-heavy environments [31, 32, 10].

To address these challenges, we draw inspiration from Schrödinger’s thought experiment on uncertainty and propose **Schrödinger’s Navigator**, a principled navigation framework that treats unobserved space as a superposition of plausible future worlds and reasons over them before committing to an action, as illustrated in Figure 1. Unlike prior approaches [35, 7, 10] that assume a single, fixed completion of the partially observed environment, Schrödinger’s Navigator explicitly imagines how the world could evolve along multiple candidate trajectories and leverages these *imagined futures* to guide decision-making.

By planning over a distribution of possible scene configurations, the agent effectively reasons “beyond” current occlusions, anticipating potential risks and plausible target locations in regions that have not yet been directly observed. This belief-aware planning paradigm enables more robust and cautious navigation behavior in cluttered, uncertain environments, where prematurely committing to a single interpretation of the world can lead to irreversible failures.

At its core, Schrödinger’s Navigator builds on a trajectory-conditioned 3D world model [23], but departs fundamentally from prior world-model-based navigation approaches [2, 41, 15] in how imagined futures are generated, selected, and exploited for planning. Rather than predicting a single global rollout or committing to a fixed completion of the partially observed scene, the model conditions future predictions on a diverse set of candidate trajectories. Given egocentric visual observations and sampled trajectories, it generates hypothetical 3D views corresponding to what the agent would perceive along each path, thereby maintaining a superposition of plausible realizations of the unobserved space, an operational analogue of Schrödinger’s thought experiment.

To efficiently explore possible futures, we introduce an *adaptive, occluder-aware trajectory sampling* strategy that focuses on regions with high uncertainty or occlusion. This avoids the uniform or dense sampling used in prior world-model navigation methods, which can be computationally expensive and insensitive to occlusion structure.

The resulting trajectory-conditioned 3D predictions are spatially aligned, fused, and integrated into the navigation map to construct a *Future-Aware Value Map* (FAVM). Unlike conventional value maps derived solely from observed states or single-step predictions, FAVM explicitly aggregates evidence from multiple imagined futures and assigns value to currently unobserved regions based on their anticipated utility and

risk. This enables the navigation policy to select actions that proactively reduce uncertainty, reason about occluded targets, and avoid hazardous regions, without requiring dense global reconstruction or additional exploratory detours.

We evaluate Schrödinger’s Navigator in both the Habitat simulator and on the real-world physical Go2 quadruped robot across challenging scenarios involving severe static occlusions and latent hazards. Across all settings, Schrödinger’s Navigator consistently outperforms or matches strong zero-shot object navigation baselines, while demonstrating markedly improved robustness in self-localization and object localization. These results highlight the effectiveness of explicitly reasoning over *trajectory-conditioned imagined 3D futures* at inference time as a scalable and generalizable alternative to conventional world-model navigation under real-world uncertainty.

In summary, we make the following contributions:

- We identify a fundamental limitation of existing zero-shot object navigation methods in realistic, cluttered environments: their reliance on a single inferred scene interpretation without explicitly reasoning over uncertainty and occluded space.
- We propose **Schrödinger’s Navigator**, a belief-aware navigation framework that treats unobserved regions as a superposition of plausible future worlds and plans by reasoning over multiple *trajectory-conditioned imagined 3D futures* at inference time.
- We introduce an *adaptive, occluder-aware trajectory sampling* strategy that focuses imagination on geometrically and semantically uncertain regions, enabling efficient exploration without dense global reconstruction.
- We develop a *Future-Aware Value Map* (FAVM) that aggregates evidence from multiple imagined futures to assign value to currently unobserved space, allowing the agent to proactively mitigate occlusions, reduce risk, and uncover hidden targets.

II. RELATED WORK

Object Navigation (ObjectNav) [13] studies embodied agents that must locate a target object in unseen environments. *Task-trained* approaches based on reinforcement/imitation learning [35, 7, 27, 34] rely on large-scale training and often generalize poorly to cluttered real-world scenes, making sim-to-real deployment challenging. *Zero-shot* approaches instead leverage pretrained vision-language models [22, 26, 12] or large language models [44, 52, 36] to perform reasoning and planning without task-specific training [45, 12, 36]. These methods progressively enhance semantics-driven exploration and planning through multimodal target embeddings [26, 12], vision-language frontier maps [45], instruction-based prompting [25, 52], and adaptive fusion of semantic and geometric cues [20, 14, 8, 49, 48]. Despite progress, zero-shot ObjectNav remains brittle in realistic, occlusion-heavy environments and under unknown risks [12, 45], as value estimation is dominated by visible frontiers and lacks explicit reasoning about what lies behind occluders, leading to myopic exploration.

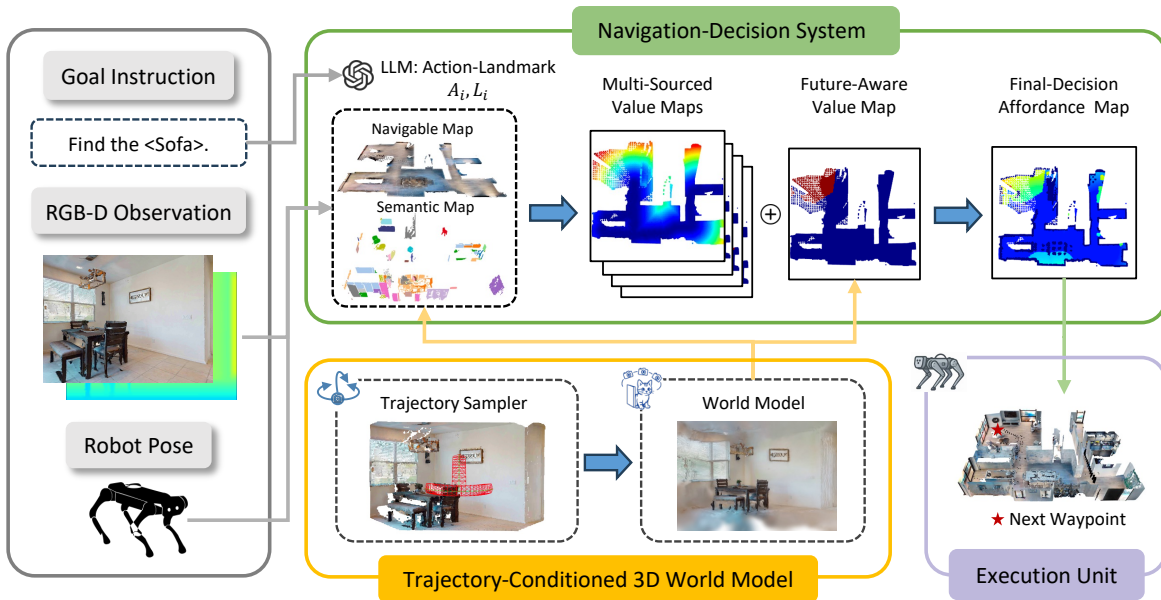


Fig. 2: Overview of our Navigator pipeline. Left: The system receives a goal instruction, RGB-D observations, and the robot pose as input. Bottom center: A trajectory sampler adaptively generates three candidate trajectories and conditions a 3D world model. The model predicts future 3DGS observations along these trajectories—left bypass, right bypass, and over-the-top—to infer occluded and unobserved regions. Top right: The predicted cues are fused with current observations to construct and update multi-sourced value maps and enable future-aware reasoning. This process produces a final affordance map used for intermediate waypoint selection. Bottom right: The execution unit follows the selected waypoint and generates control commands to navigate the robot continuously toward the goal.

Imagination for Navigation leverages generative or predictive models to simulate future observations and inform planning [19, 2, 30, 41]. Related model-based RL and world-model approaches learn predictive dynamics models, rolling out trajectories in latent space to train policies [24, 40]. Recent navigation world models extend this idea to egocentric visual streams: NWM [2] uses a conditional diffusion transformer to predict future trajectories and views in pixel space and rank candidate paths, while NavigateDiff [30] employs diffusion-based visual prediction as a zero-shot navigation assistant. Language-conditioned variants provide guidance by generating images of instruction landmarks and by imagining instruction-conditioned future views whose alignment yields planning values for action selection, as in VISTA and VISTA_{v2} [28, 16, 15]. Other works learn scene imagination modules or predictive occupancy maps to complete unobserved spaces and facilitate exploration [18, 38, 37]. Unlike prior works, Schrödinger’s Navigator imagines future observations along multiple candidate paths with a trajectory-conditioned 3D world model, creating a Future-Aware Value Map (FAVM). This map reasons about occlusions and risks to locate blind-spot targets for robust zero-shot navigation.

III. METHOD

We introduce **Schrödinger’s Navigator** (Figure 2), a framework for reducing occlusion-induced uncertainty in zero-shot navigation. Using a trajectory-conditioned 3D world model, it

generates plausible future observations along candidate paths to reason about unobserved regions.

A. Problem Definition

We study zero-shot object navigation (ZSON) in previously unseen 3D environments with heavy occlusions and inherent environmental uncertainties. An embodied agent operates in an environment \mathcal{E} and is given a goal instruction I that specifies a target object category (e.g., “Finding the cat”). At each decision step t , the agent is at an unknown global state $x_t \in \mathcal{X}$ but only has access to an egocentric observation

$$O_t = \{V_t, D_t, P_t\}, \quad (1)$$

where V_t is the current RGB image, D_t is the depth map from the onboard RGB-D sensor, and P_t is the robot pose in the world coordinate frame. Large portions of the environment, including the target object and potential hazards, may lie in unobserved or occluded regions that are not directly visible in O_t . An episode terminates successfully when the target object is within a small distance threshold and lies in the robot’s field of view, or ends in failure if a maximum step budget is exceeded or the robot enters unsafe regions.

Our goal is to develop a navigation framework that reasons about unobserved space, predicts plausible futures behind occluders, and selects safe, informative trajectories to enable successful object discovery in complex real-world environments.

B. Trajectory-Conditioned 3D World Model

1) *Adaptive Occluder-Aware Trajectory Sampling*: To achieve obstacle avoidance and target localization using a world model, we propose an adaptive occluder-aware trajectory sampling strategy. Since imagining a single path often fails to detect occluded hazards, our method generates diverse candidate trajectories to explicitly probe unobserved regions. By extracting occluder boundaries from real-time depth observations, we dynamically adjust orbit parameters to align with scene geometry, ensuring the generated paths are both physically plausible and visually informative.

To make the imagined outcomes more predictive, we select three candidate trajectories, along which cameras orbit around the obstacle: (1) a left-bypass path, (2) a right-bypass path, and (3) an over-the-top path. This trajectory selection plan ensures sufficient coverage of occluded areas while maintaining an acceptable computational budget, preventing excessive latency.

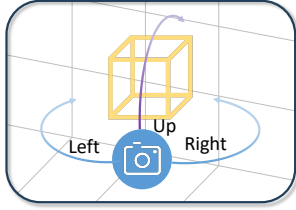


Fig. 3: Sampling the camera trajectory around the obstacle to maximize field of view coverage.

Figure 3 shows our trajectory generation with the set of trajectory types $\mathcal{V}=\{L, U, R\}$. For each $v \in \mathcal{V}$, a unified trajectory generator $\mathcal{F}(\cdot)$ outputs a trajectory $\mathcal{T}^{(v)}$:

$$\mathcal{T}^{(v)} = \mathcal{F}(v, \mathbf{K}, N_{pose}, d_v, d_c), \quad (2)$$

where \mathbf{K} is the intrinsic parameter, N_{pose} is the number of camera poses, d_v is the total length of trajectory v , and d_c is the distance between the camera center and the orbit center.

Occluder Boundary Estimation. Using the current depth and pose, we build a local point cloud and remove ground points to isolate obstacles. We then cluster the remaining points and, within the forward sector, select a primary occluder \mathcal{O}_t based on larger projected occupancy, shorter distance, and better alignment with the forward direction. Finally, we project \mathcal{O}_t onto the ground plane and extract its boundary \mathcal{B}_t using either a convex-hull algorithm [3] or an alpha-shape method [11] suitable for complex non-convex structures.

Orbit Center and Clearance. We define the orbit center c_t as the centroid of the boundary \mathcal{B}_t : $c_t = \frac{1}{|\mathcal{B}_t|} \sum_{b \in \mathcal{B}_t} b$. The effective obstacle radius is estimated as $r_t = \max_{b \in \mathcal{B}_t} \|b - c_t\|_2$. To determine the safe orbital distance d_c , we calculate:

$$d_c = \max(r_t + r_{robot} + \delta, d_c^{\min}), \quad (3)$$

where δ is a safety margin and d_c^{\min} prevents the formation of degenerate orbits around small debris.

Boundary-Aligned Angular Span. To ensure the trajectories provide meaningful observations of the occluded region, we adapt the arc length based on the angular span of the obstacle. For every boundary point $b \in \mathcal{B}_t$, we compute its azimuth $\theta(b)$ relative to c_t . Unwrapping these angles yields the occluder span $[\theta_{\min}, \theta_{\max}]$. We expand this span by $\Delta\theta$ to ensure the camera “peeks” past the edge:

$$\theta_L = \theta_{\max} + \Delta\theta, \quad \theta_R = \theta_{\min} - \Delta\theta. \quad (4)$$

Let θ_0 be the agent’s current azimuth relative to c_t . The required arc lengths for the Left and Right bypasses are derived from the angular displacement along the clearance circle:

$$d_v^{(L)} = \text{clamp}(d_c \cdot |\text{wrap}(\theta_L - \theta_0)|, d_v^{\min}, d_v^{\max}), \quad (5)$$

$$d_v^{(R)} = \text{clamp}(d_c \cdot |\text{wrap}(\theta_R - \theta_0)|, d_v^{\min}, d_v^{\max}), \quad (6)$$

where $\text{wrap}(\cdot)$ computes signed shortest angular difference. The upper bound d_v^{\max} is synchronized with N_{pose} and the step size of $\mathcal{F}(\cdot)$ to respect compute budget of the world model.

Trajectory Instantiation. Based on these parameters, the set \mathcal{V} is instantiated as follows:

- **Left/Right (Tangential Orbit):** For $v \in \{L, R\}$, we uniformly sample N_{pose} poses along the angular arc $[\theta_0, \theta_v]$ at radius d_c . The camera yaw is constrained to look at c_t , generating smooth, pose-continuous orbits that maintain a stable reference while keeping the occluder boundary in view.
- **Up (Over-the-Top):** We align the trajectory horizontally to the midpoint of the occlusion span, $\theta_U = \frac{1}{2}(\theta_{\min} + \theta_{\max})$. The arc length $d_v^{(U)}$ is clamped similarly to the lateral paths. We superimpose a smooth elevation curve (peaking at h_{\max}) onto the horizontal arc, optionally applying a pitch-down tilt proportional to the lift to maintain near-field visibility.

2) *World Model for Future Imagination*: Given each generated trajectory $\mathcal{T}^{(v)}$, we use a world model to generate future imaginations that are geometrically consistent. We adopt *FlashWorld* [23] as the backend for future scene imagination due to its ability to produce high-quality, 3D-consistent 3D Gaussian Splatting (3DGS) scenes within seconds. Unlike conventional 3D Gaussian representations, we encode each Gaussian as a nine-dimensional vector $\mathbf{g} = [x, y, z, r, g, b, rad, opa, label]$, which substantially reduces memory footprint and accelerates downstream processing while preserving sufficient expressive power. However, *FlashWorld* is an affine-invariant world model and cannot directly generate scenes aligned with the environment’s metric scale. To produce high-quality scenes that are also metrically consistent, we perform the following two-step alignment:

(1) *Coordinate System Transformation.* To generate high-quality future scenes, we construct a local coordinate system \mathcal{W} centered at the current observation frame to match the generated trajectories to the trajectory distribution preferred by the world model as closely as possible. After generating the

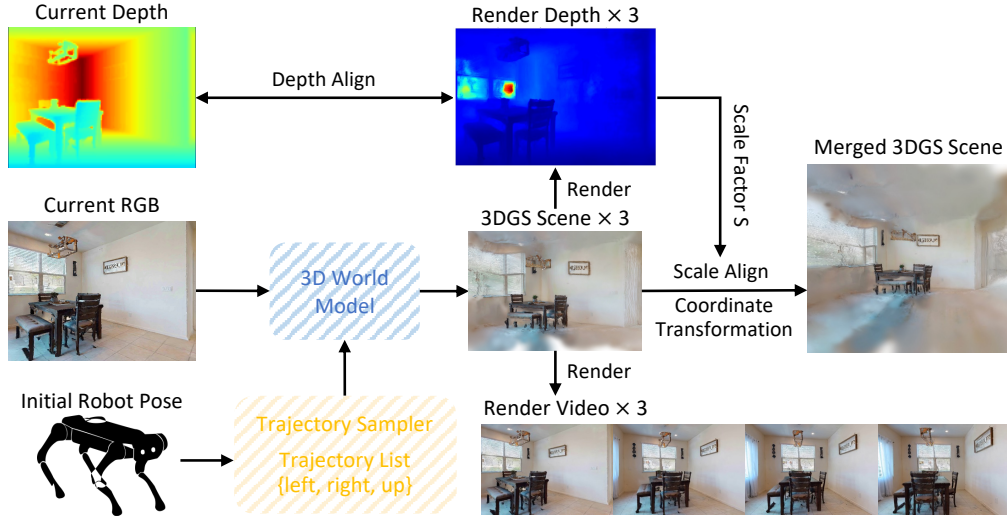


Fig. 4: Overview of trajectory-conditioned 3D world model. Given the current RGB frame and the initial robot pose, a trajectory sampler produces a set of adaptive occluder-aware candidate camera trajectories (left, right, up). These trajectories are then used to condition a 3D world model that predicts a 3DGS scene for each candidate. From the predicted scenes, we render short RGB videos and their corresponding depth maps. The rendered depths are then aligned with the current depth observation to estimate a global scale factor s , which is subsequently used to consistently scale and align the predicted 3DGS scenes. The aligned scenes are finally transformed into the world coordinate frame and fused into a single merged 3DGS scene that is geometrically and visually consistent with the robot’s current observation.

future scene, we transform the scene from the local coordinate system $\hat{\mathcal{W}}$ back to the global world coordinate system \mathcal{W} .

(2) *Global Scale Alignment.* To merge the generated scene back into the original environment, we estimate a global scale factor s that aligns the scale of the generated scene with the metric scale. Specifically, given the metric depth D^{gt} of the current observation obtained from the RGB-D camera and the rendered depth D^{gs} of the corresponding frame in the generated scene, we compute s as follows:

$$s = \text{median}_{p \in \Omega} \left(\frac{D^{\text{gt}}(p)}{D^{\text{gs}}(p)} \right), \quad (7)$$

where p denotes a pixel location in the image plane and Ω denotes the set of valid pixels for which both the metric depth $D^{\text{gt}}(p)$ and the generated-scene depth $D^{\text{gs}}(p)$ are available. The ratio between the median of the metric depth and the median of the rendered depth over Ω provides a robust estimate of the global scale.

Semantic Label Transfer. To enrich aligned 3DGS scene with semantic information, we lift 2D semantic predictions from the image plane to the Gaussian primitives. Given the current RGB frame I and the camera intrinsics K , we apply an off-the-shelf semantic segmentation network to obtain a per-pixel semantic map $S(p) \in \{1, \dots, C\}$ over the image domain Ω_{img} , where C denotes the number of semantic categories and $p = (u, v)$ indexes pixel locations.

Let $\mathbf{x}_i \in \mathbb{R}^3$ denote the 3D center of the i -th Gaussian in the (scale-aligned) camera coordinate frame, and let $\pi(\cdot)$ be the

pinhole projection function. We project each Gaussian center onto the image plane as

$$p_i = \pi(K \mathbf{x}_i), \quad p_i \in \mathbb{R}^2. \quad (8)$$

If p_i lies within the image bounds and admits a valid semantic prediction, we assign the corresponding pixel-level label to the Gaussian by

$$\ell_i = S(p_i), \quad (9)$$

where ℓ_i denotes the semantic label stored in the label field of the i -th Gaussian.

To avoid spurious assignments from occluded or invalid projections, we restrict the transfer to Gaussians whose projected pixels lie within the valid depth region Ω and satisfy a depth-consistency check with the rendered 3DGS depth, i.e., $|D^{\text{gs}}(p_i) - D^{\text{gt}}(p_i)| < \tau_d$. We accumulate these assignments across multiple views and fuse them via majority voting to produce a robust semantic label for each Gaussian. This projection-and-transfer process results in a semantically annotated 3DGS scene, where each visible Gaussian primitive inherits a semantic category from 2D segmentation.

C. Future-Aware Navigation Decision

1) *Construction of Future-Aware Value Map (FAVM):* To move beyond purely myopic, observation-only decisions, we augment the navigation pipeline with a **Future-Aware Value Map (FAVM)**, constructed from imagined 3DGS scenes. These augmented maps extend the currently observed scene with hypothesized free space and semantic entities behind occluders.

We then formally define the FAVM, denoted as m_{FA} , which directly scores each navigable Gaussian by jointly accounting for semantic relevance and information gain inferred from these imagined futures. For each navigable Gaussian $g \in \mathcal{G}_{\text{nav}}$ with 3D center $\mathbf{x}_g \in \mathbb{R}^3$, we define:

$$m_{\text{FA}}(g) = \alpha_{\text{sem}} S(g) + \alpha_{\text{exp}} E(g), \quad (10)$$

where $S(g)$ is the semantic score, $E(g)$ is the exploration score, and $\alpha_{\text{sem}}, \alpha_{\text{exp}} > 0$ are weighting coefficients.

Semantic score $S(g)$: target proximity. We focus on Gaussians whose semantic labels match the target category (e.g., cat, table). Let $\mathcal{T}_{\text{real}}$ denote target Gaussians obtained from direct observations and \mathcal{T}_{hyp} denote target-like Gaussians hypothesized by the world model (e.g., a cat inferred to be behind a table). For any set \mathcal{S} , we define the distance from g to \mathcal{S} as $d(g, \mathcal{S}) = \min_{g' \in \mathcal{S}} \|\mathbf{x}_g - \mathbf{x}_{g'}\|_2$. The semantic score $S(g)$ is designed to increase when g is closer to either real or hypothesized targets. We additionally apply a discount factor $\lambda_{\text{sem}} < 1$ to \mathcal{T}_{hyp} so that imagined targets contribute less than directly observed ones.

Exploration score $E(g)$: coverage of new free space. Let $\mathcal{F}_{\text{new}} \subset \mathcal{G}_{\text{nav}}$ denote Gaussians corresponding to free space predicted by the world model but not yet observed. For each candidate g , we consider a visibility radius r_{vis} and count how many newly predicted free Gaussians lie in its local neighborhood:

$$\tilde{E}(g) = \sum_{g' \in \mathcal{F}_{\text{new}}} \mathbb{I}[\|\mathbf{x}_{g'} - \mathbf{x}_g\|_2 \leq r_{\text{vis}}]. \quad (11)$$

We normalize $\tilde{E}(g)$ to obtain $E(g) \in [0, 1]$. Intuitively, positions that reveal more previously unseen yet likely free regions receive higher exploration scores.

2) *Fusion with Observation-Based Cues:* While the FAVM provides foresight, reliable navigation requires grounding in reality using cues from current observations. We represent this ground truth using a *Multi-sourced Value Map* m , which aggregates action preferences (m_a), semantic landmarks (m_s), trajectory constraints (m_t), and heuristic guidance (m_i):

$$m = m_a + m_s + m_t + m_i. \quad (12)$$

Detailed mathematical definitions and calculation procedures for each component map (i.e., m_a, m_s, m_t, m_i) are provided in Appendix B. Crucially, m and m_{FA} capture complementary information: the former focuses on visible certainties and instruction following, while the latter encodes semantic and exploratory value inferred from imagined futures.

To enable robust decision-making, we fuse them into a final decision affordance map m_{aff} :

$$m_{\text{aff}}(g) = \beta m(g) + (1 - \beta) m_{\text{FA}}(g), \quad g \in \mathcal{G}_{\text{nav}}, \quad (13)$$

where $\beta \in [0, 1]$ balances current-step evidence and future-aware reasoning. In the target selection step, we select the optimal waypoint p^* by maximizing the affordance map:

$$p^* = \arg \max_{p \in m_{\text{aff}}} m_{\text{aff}}(p). \quad (14)$$

This yields a compact, single future-aware map that simultaneously encodes semantic goal guidance, information gain, and safety.

3) *Waypoint Selection and Execution:* The guidance signals for the observation-based map m (specifically m_a and m_s) are derived from a hierarchical planner. Following *InstructNav* [25], we employ a large language model (LLM) to parse the natural language instruction I into a sequence of action-landmark pairs, termed DCoN.

At each decision step t , given the current observation $O_t = \{V_t, D_t, P_t\}$ and the accumulated plan $C_{1:t}$, the LLM predicts the next pair $(a_{t+1}, \ell_{t+1}) = f_{\text{LLM}}(I, C_{1:t}, O_t)$. This high-level plan directs the construction of m , which is then fused with our proposed FAVM to determine the final waypoint p^* . The selected waypoint is finally fed to a local planner to generate high-frequency velocity commands between decision steps.

IV. EXPERIMENTS

In this section, we evaluate Schrödinger’s Navigator in both simulation environments and complex real-world scenarios. We aim to verify that our future-aware reasoning capability improves robustness against severe occlusions and environmental uncertainties compared to standard ZSON baselines.

A. Experimental Setup

1) *Baselines:* We compare our approach against a broad set of strong baselines, including task-trained approaches (ZSON [26], PixNav [4], SPNet [51], SGM [49]), zero-shot geometric or semantic explorers (CoW [12], ESC [52], L3MVN [46], TriHelper [47], VoroNav [43], GAMap [14]), and LLM-based planners (VLFM [45], InstructNav [25], ApexNav [48], CogNav [5]). In particular, InstructNav* denotes a modified version of InstructNav in which we replace the original LLM and VLM with GPT-4o, and use 3D Gaussian representations instead of raw point clouds throughout the pipeline to improve computational efficiency. Detailed descriptions of baselines are provided in the Appendix C.

2) Implementation Details:

a) *System Configuration:* For high-level reasoning, we employ GPT-4o [17] to parse goal instructions and judge navigation directions. For future imagination, we utilize FlashWorld [23] to generate 3D-consistent 3DGS scenes. Semantic segmentation is performed using GLEE [42]. In deployment, we do not invoke the world model at every decision step. Instead, we trigger imagination periodically or when occlusion is high. All large model parameters are kept at default settings. A comprehensive list of all hyperparameters, including the specific geometric constraints for trajectory sampling (e.g., N_{pose}, δ) and coefficients for value map fusion, is provided in Appendix A.

b) *Computation:* All simulation experiments and server-side inferences for real-world deployment are conducted on a single compute node. The simulation runs on two NVIDIA RTX 4090 GPUs, while the real-world inference is accelerated by a single NVIDIA H800 GPU.

B. Simulation Evaluation

1) *Dataset and Metrics*: We perform large-scale evaluation on the HM3D benchmark [33] within the Habitat simulator [29]. HM3D comprises 36 high-fidelity reconstructed indoor scenes (residential and commercial). We evaluate across 1,000 episodes covering six common target categories. We adopt three standard metrics: (1) **Success Rate (SR)**: The fraction of episodes where the agent stops within a fixed threshold ($d \leq \tau$) of the target. (2) **Success weighted by Path Length (SPL)**: A rigorous metric balancing success and path efficiency. (3) **Distance to Goal (DTG)**: The geodesic distance to the target at termination. DTG is particularly critical for analyzing failure cases in occluded scenes, as it indicates how close the agent could get to the hidden target.

TABLE I: **Quantitative Comparison on Simulation Results.** Cell background colors indicate the method is the **best**, **second best**, or **third best** on this metric.

| Method | Training Free | HM3D | | |
|------------------|---------------|---------------|----------------|------------------|
| | | SR \uparrow | SPL \uparrow | DTG \downarrow |
| ZSON [26] | ✗ | 0.255 | 0.126 | – |
| PixNav [4] | ✗ | 0.379 | 0.205 | – |
| SPNet [51] | ✗ | 0.312 | 0.101 | – |
| SGM [49] | ✗ | 0.602 | 0.308 | – |
| ESC [52] | ✓ | 0.392 | 0.223 | – |
| VLFM [45] | ✓ | 0.525 | 0.304 | – |
| VoroNav [43] | ✓ | 0.420 | 0.260 | – |
| L3MVN [46] | ✓ | 0.504 | 0.231 | 4.43 |
| TriHelper [47] | ✓ | 0.565 | 0.253 | 3.87 |
| GAMap [14] | ✓ | 0.531 | 0.260 | – |
| InstructNav [25] | ✓ | 0.510 | 0.187 | 2.89 |
| InstructNav* | ✓ | 0.453 | 0.186 | 3.38 |
| CogNav [5] | ✓ | 0.725 | 0.262 | – |
| ApexNav [48] | ✓ | 0.762 | 0.380 | – |
| Ours | ✓ | 0.739 | 0.317 | 2.23 |

2) *Quantitative Results*: Table I summarizes the performance on HM3D. Our Schrödinger’s Navigator demonstrates competitive performance compared to state-of-the-art baselines. Notably, our method achieves the best performance in terms of DTG (2.23). This indicates that while strict success (SR) is capped by safety protocols in cluttered environments, FAVM successfully navigates the agent closer to the target than any other method, validating its superior geometric reasoning.

While recent methods such as ApexNav [48] and CogNav [5] improve SR and SPL using adaptive exploration or cognitive modeling for global reasoning, our approach is designed for occlusion-heavy scenarios, where approaching hidden targets often takes priority over following the shortest path. To uncover blind spots, our trajectory sampling introduces exploratory detours around obstacles, allowing the agent to “see” behind occluders and achieve a state-of-the-art DTG (2.23). These detours, however, increase the total path length and cumulative error in large-scale benchmarks, creating a trade-off between exploration for occlusion handling and strict success metrics (SR/SPL).

TABLE II: Ablation analysis on trajectory ensemble size N and the fusion coefficient β . We report Success Rate (SR) and imagination latency per trigger.

| Method Variant | SR \uparrow | Imag. Latency (s) |
|---|---------------|-------------------|
| Baseline (No Imag) | 0.453 | – |
| Single Trajectory ($N = 1$) | 0.542 | 8 |
| Dense Sampling ($N = 5$) | 0.674 | 40 |
| Imagination-Heavy ($\beta = 0.2$) | 0.380 | 24 |
| Observation-Heavy ($\beta = 0.8$) | 0.695 | 24 |
| Ours ($N = 3, \beta = 0.5$) | 0.739 | 24 |

3) *Ablation Analysis*: To disentangle the performance gains of Schrödinger’s Navigator and validate our design choices—specifically the *Adaptive Occluder-Aware Sampling* strategy and the *Future-Aware Value Map* (FAVM), we compared our full model against two distinct sets of variants:

- **Impact of Trajectory Ensemble Size (N)**: To verify that $N = 3$ represents the optimal trade-off between topological coverage and efficiency, we varied the number of imagined trajectories: (1) $N = 1$ (*Single*), which samples a trajectory at the occluder’s center; (2) $N = 3$ (*Ours*); and (3) $N = 5$ (*Dense*), which adds two interpolated trajectories between the tangents and the center.
- **Sensitivity of Fusion Coefficient (β)**: We analyzed the impact of the balancing parameter β in Equation 13, which governs the trade-off between trusting current observations versus following imagined guidance. We compared imagination-heavy ($\beta = 0.2$), balanced ($\beta = 0.5$, Ours), and observation-heavy ($\beta = 0.8$) configurations.

The results, shown in Table II provide quantitative validation for our design choices, highlighting the critical balance between exploration capability, computational efficiency, and trust in generative predictions. First, the necessity of imagination is evident as our method outperforms the *No-Imagination* baseline by 28.6% in success rate. This substantial gain confirms that reasoning about occluded spaces is essential to prevent myopic behaviors in cluttered environments.

Our analysis of the trajectory ensemble size identifies a clear peak in performance at $N = 3$. While a single trajectory ($N = 1$) raises SR to 0.542, it remains 9.7% lower than our tri-trajectory ensemble, as limited viewpoints often fail to resolve occlusions. Denser sampling ($N = 5$) yields no further benefit, slightly dropping SR to 0.674 while incurring a prohibitive 40s latency. We hypothesize that dense sampling introduces redundant or noisy geometric cues that confuse the agent.

Finally, the ablation on the fusion coefficient β highlights the importance of regulating the fusion ratio between imagination and real-world observations. Heavily relying on imagination ($\beta = 0.2$) results in a performance collapse, dropping the SR to 0.380, falling even below the *No-Imagination* baseline. This indicates that unchecked generative predictions can actively mislead the agent. Conversely, suppressing imagination ($\beta = 0.8$) limits foresight, resulting in a lower 0.695 SR.



Fig. 5: Real-world navigation demonstrations of Schrödinger’s Navigator. This figure highlights multi-robot navigation capabilities for static objects across three distinct indoor scenarios: (a) an Office “Chair”, (b) a Classroom “Plant”, and (c) a Common Room “Trash Can”. For each scenario, the top row illustrates the third-person view of the navigation trajectory. The middle row presents the robot’s egocentric perspective, where the yellow dashed line indicates the predicted direction and the orange box frames the target object. The bottom row visualizes the corresponding scenes as imagined by the system’s world model during navigation, with the orange box in these scenes showing the imagined appearance of the target object.

The balanced configuration ($\beta = 0.5$) achieves the highest SR of 0.739, demonstrating that robust navigation relies on grounding generative guidance with real-world observations.

C. Real-World Deployment

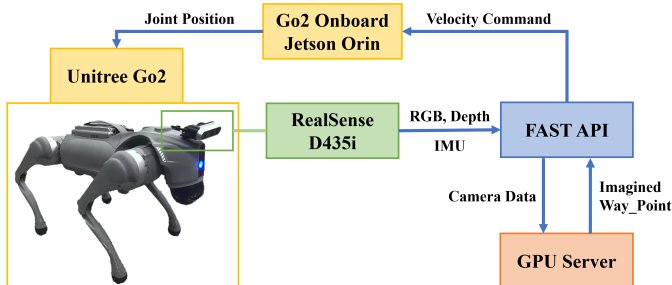


Fig. 6: System setup for experiments.

1) Platform and Environments:

a) *Hardware Platform*: We deploy our system on a Unitree Go2 quadruped robot equipped with a RealSense D435i camera (640×480 , 69.4° HFoV) for synchronized RGB-D and IMU data capture. The robot communicates with the remote GPU server via a FastAPI interface.

b) *Scenarios*: As show in Figure 5, we established a rigorous benchmark across three distinct indoor environments: *Office*, *Classroom*, and *Common Room*. We designed navigation tasks under two conditions to test adaptability: (1) **Static Object Search**: Standard search tasks for objects like chairs or plants, requiring the agent to explore and locate targets. (2) **Scenarios with Unknown Risks**: Environments containing severe static occlusions that are not visible from a distance.

These scenarios specifically test the agent’s ability to anticipate uncertainty and avoid getting stuck in local optima or blind spots.

TABLE III: Real-world quantitative comparison against the InstructNav* baseline. We report success counts (Success / Total Trials) across three indoor environments.

| Scene | Office | Classroom | Common Room | All |
|-------------------------------------|--------|-----------|-------------|-------|
| Search for static objects | | | | |
| InstructNav* | 7/10 | 7/10 | 8/10 | 22/30 |
| Ours | 8/10 | 8/10 | 7/10 | 23/30 |
| Scenarios with Unknown Risks | | | | |
| InstructNav* | 4/10 | 3/10 | 4/10 | 11/30 |
| Ours | 5/10 | 6/10 | 6/10 | 17/30 |

2) *Performance Analysis*: As shown in Table III, we report success counts over 30 total trials.

- **Search for static objects**: Our method consistently outperforms the baseline InstructNav*. In standard static search tasks, we achieve comparable high success rates (23/30 vs. 22/30).
- **Scenarios with Unknown Risks**: The advantage of Schrödinger’s Navigator becomes pronounced in complex scenarios involving unknown risks. In these challenging tasks, our method achieves a success rate of (17/30), surpassing InstructNav* (11/30), whose performance degrades markedly when facing unexpected occlusions.

These results validate that reasoning over imagined 3D futures allows the robot to proactively avoid risky regions and

discover targets in blind spots, capabilities that are crucial for robust real-world deployment. Qualitative demonstrations are provided in Figure 5.

V. CONCLUSION

Schrödinger’s Navigator addresses ZSON limitations in occluded environments by leveraging a trajectory-conditioned world model to imagine and fuse plausible 3D futures into a unified scene. This training-free framework constructs a single affordance map encoding semantics, exploration, and safety. Real-world experiments on a Unitree Go2 demonstrate its robustness, matching baselines in static tasks while significantly outperforming them in complex, dynamic scenarios.

REFERENCES

- [1] Peter Anderson, Angel Chang, Devendra Singh Chaplot, Alexey Dosovitskiy, Saurabh Gupta, Vladlen Koltun, Jana Kosecka, Jitendra Malik, Roozbeh Mottaghi, Manolis Savva, et al. On evaluation of embodied navigation agents. *arXiv preprint arXiv:1807.06757*, 2018.
- [2] Amir Bar, Gaoyue Zhou, Danny Tran, Trevor Darrell, and Yann LeCun. Navigation world models. In *Proceedings of the Computer Vision and Pattern Recognition Conference*, pages 15791–15801, 2025.
- [3] C Bradford Barber, David P Dobkin, and Hannu Huudanpaa. The quickhull algorithm for convex hulls. *ACM Transactions on Mathematical Software (TOMS)*, 22(4): 469–483, 1996.
- [4] Wenzhe Cai, Siyuan Huang, Guangran Cheng, Yuxing Long, Peng Gao, Changyin Sun, and Hao Dong. Bridging zero-shot object navigation and foundation models through pixel-guided navigation skill. In *2024 IEEE International Conference on Robotics and Automation (ICRA)*, pages 5228–5234. IEEE, 2024.
- [5] Yihan Cao, Jiazhao Zhang, Zhinan Yu, Shuzhen Liu, Zheng Qin, Qin Zou, Bo Du, and Kai Xu. Cognav: Cognitive process modeling for object goal navigation with llms. In *Proceedings of the IEEE/CVF International Conference on Computer Vision*, pages 9550–9560, 2025.
- [6] Devendra Singh Chaplot, Dhiraj Gandhi, Saurabh Gupta, Abhinav Gupta, and Ruslan Salakhutdinov. Learning to explore using active neural slam. *arXiv preprint arXiv:2004.05155*, 2020.
- [7] Devendra Singh Chaplot, Dhiraj Prakashchand Gandhi, Abhinav Gupta, and Russ R Salakhutdinov. Object goal navigation using goal-oriented semantic exploration. *Advances in Neural Information Processing Systems*, 33: 4247–4258, 2020.
- [8] Junting Chen, Guohao Li, Suryansh Kumar, Bernard Ghanem, and Fisher Yu. How to not train your dragon: Training-free embodied object goal navigation with semantic frontiers. *arXiv preprint arXiv:2305.16925*, 2023.
- [9] Kevin Chen, Juan Pablo De Vicente, Gabriel Sepulveda, Fei Xia, Alvaro Soto, Marynel Vázquez, and Silvio Savarese. A behavioral approach to visual navigation with graph localization networks. *arXiv preprint arXiv:1903.00445*, 2019.
- [10] Vishnu Sashank Dorbala, Bhrij Patel, Amrit Singh Bedi, and Dinesh Manocha. Right place, right time! generalizing objectnav to dynamic environments with portable targets (p-objectnav). *arXiv preprint arXiv:2403.09905*, 2024.
- [11] Herbert Edelsbrunner, David Kirkpatrick, and Raimund Seidel. On the shape of a set of points in the plane. *IEEE Transactions on information theory*, 29(4):551–559, 2003.
- [12] Samir Yitzhak Gadre, Mitchell Wortsman, Gabriel Ilharco, Ludwig Schmidt, and Shuran Song. Cows on pasture: Baselines and benchmarks for language-driven zero-shot object navigation. In *Proceedings of the IEEE/CVF Conference on Computer Vision and Pattern Recognition*, pages 23171–23181, 2023.
- [13] Saurabh Gupta, James Davidson, Sergey Levine, Rahul Sukthankar, and Jitendra Malik. Cognitive mapping and planning for visual navigation. In *Proceedings of the IEEE conference on computer vision and pattern recognition*, pages 2616–2625, 2017.
- [14] Hao Huang, Yu Hao, Congcong Wen, Anthony Tzes, Yi Fang, et al. Gamap: Zero-shot object goal navigation with multi-scale geometric-affordance guidance. *Advances in Neural Information Processing Systems*, 37: 39386–39408, 2024.
- [15] Yanjia Huang, Xianshun Jiang, Xiangbo Gao, Mingyang Wu, and Zhengzhong Tu. Vistav2: World imagination for indoor vision-and-language navigation. *arXiv preprint arXiv:2512.00041*, 2025.
- [16] Yanjia Huang, Mingyang Wu, Renjie Li, and Zhengzhong Tu. Vista: Generative visual imagination for vision-and-language navigation. *arXiv preprint arXiv:2505.07868*, 2025.
- [17] Aaron Hurst, Adam Lerer, Adam P Goucher, Adam Perelman, Aditya Ramesh, Aidan Clark, AJ Ostrow, Akila Welihinda, Alan Hayes, Alec Radford, et al. Gpt-4o system card. *arXiv preprint arXiv:2410.21276*, 2024.
- [18] Kapil Katyal, Katie Popek, Chris Paxton, Phil Burlina, and Gregory D Hager. Uncertainty-aware occupancy map prediction using generative networks for robot navigation. In *2019 International Conference on Robotics and Automation (ICRA)*, pages 5453–5459. IEEE, 2019.
- [19] Jing Yu Koh, Honglak Lee, Yinfei Yang, Jason Baldridge, and Peter Anderson. Pathdreamer: A world model for indoor navigation. In *Proceedings of the IEEE/CVF International Conference on Computer Vision*, pages 14738–14748, 2021.
- [20] Yuxuan Kuang, Hai Lin, and Meng Jiang. Openfinnav: Towards open-set zero-shot object navigation via vision-language foundation models. *arXiv preprint arXiv:2402.10670*, 2024.
- [21] Obin Kwon, Jeongho Park, and Songhwai Oh. Renderable neural radiance map for visual navigation. In *Proceedings of the IEEE/CVF Conference on Computer*

- Vision and Pattern Recognition*, pages 9099–9108, 2023.
- [22] Junnan Li, Dongxu Li, Silvio Savarese, and Steven Hoi. Blip-2: Bootstrapping language-image pre-training with frozen image encoders and large language models. In *International conference on machine learning*, pages 19730–19742. PMLR, 2023.
- [23] Xinyang Li, Tengfei Wang, Zixiao Gu, Shengchuan Zhang, Chunchao Guo, and Liujuan Cao. Flashworld: High-quality 3d scene generation within seconds. *arXiv preprint arXiv:2510.13678*, 2025.
- [24] Wei Liu, Huihua Zhao, Chenran Li, Joydeep Biswas, Billy Okal, Pulkit Goyal, Yan Chang, and Soha Pouya. X-mobility: End-to-end generalizable navigation via world modeling. In *2025 IEEE International Conference on Robotics and Automation (ICRA)*, pages 7569–7576. IEEE, 2025.
- [25] Yuxing Long, Wenzhe Cai, Hongcheng Wang, Guanqi Zhan, and Hao Dong. Instructnav: Zero-shot system for generic instruction navigation in unexplored environment. *arXiv preprint arXiv:2406.04882*, 2024.
- [26] Arjun Majumdar, Gunjan Aggarwal, Bhavika Devnani, Judy Hoffman, and Dhruv Batra. Zson: Zero-shot object-goal navigation using multimodal goal embeddings. *Advances in Neural Information Processing Systems*, 35: 32340–32352, 2022.
- [27] Bar Mayo, Tamir Hazan, and Ayellet Tal. Visual navigation with spatial attention. In *Proceedings of the IEEE/CVF conference on computer vision and pattern recognition*, pages 16898–16907, 2021.
- [28] Akhil Perincherry, Jacob Krantz, and Stefan Lee. Do visual imaginations improve vision-and-language navigation agents? In *Proceedings of the Computer Vision and Pattern Recognition Conference*, pages 3846–3855, 2025.
- [29] Xavi Puig, Eric Undersander, Andrew Szot, Mikael Dal-laire Cote, Ruslan Partsey, Jimmy Yang, Ruta Desai, Alexander William Clegg, Michal Hlavac, Tiffany Min, Theo Gervet, Vladimír Vondruš, Vincent-Pierre Berges, John Turner, Oleksandr Maksymets, Zsolt Kira, Mrinal Kalakrishnan, Jitendra Malik, Devendra Singh Chaplot, Unnat Jain, Dhruv Batra, Akshara Rai, and Roozbeh Mottaghi. Habitat 3.0: A co-habitat for humans, avatars and robots, 2023.
- [30] Yiran Qin, Ao Sun, Yuze Hong, Benyou Wang, and Ruimao Zhang. Navigatediff: Visual predictors are zero-shot navigation assistants. *arXiv preprint arXiv:2502.13894*, 2025.
- [31] Sébastien Racanière, Théophane Weber, David Reichert, Lars Buesing, Arthur Guez, Danilo Jimenez Rezende, Adrià Puigdomènech Badia, Oriol Vinyals, Nicolas Heess, Yujia Li, et al. Imagination-augmented agents for deep reinforcement learning. *Advances in neural information processing systems*, 30, 2017.
- [32] Santhosh K Ramakrishnan, Ziad Al-Halah, and Kristen Grauman. Occupancy anticipation for efficient exploration and navigation. In *European conference on computer vision*, pages 400–418. Springer, 2020.
- [33] Santhosh K Ramakrishnan, Aaron Gokaslan, Erik Wijmans, Oleksandr Maksymets, Alex Clegg, John Turner, Eric Undersander, Wojciech Galuba, Andrew Westbury, Angel X Chang, et al. Habitat-matterport 3d dataset (hm3d): 1000 large-scale 3d environments for embodied ai. *arXiv preprint arXiv:2109.08238*, 2021.
- [34] Ram Ramrakhya, Eric Undersander, Dhruv Batra, and Abhishek Das. Habitat-web: Learning embodied object-search strategies from human demonstrations at scale. In *Proceedings of the IEEE/CVF conference on computer vision and pattern recognition*, pages 5173–5183, 2022.
- [35] Ram Ramrakhya, Dhruv Batra, Erik Wijmans, and Abhishek Das. Pirlnav: Pretraining with imitation and rl finetuning for objectnav. In *Proceedings of the IEEE/CVF Conference on Computer Vision and Pattern Recognition*, pages 17896–17906, 2023.
- [36] Dhruv Shah, Błażej Osiniński, Sergey Levine, et al. Lmnav: Robotic navigation with large pre-trained models of language, vision, and action. In *Conference on robot learning*, pages 492–504. PMLR, 2023.
- [37] Hardik Shah, Jiayu Xing, Nico Messikommer, Boyang Sun, Marc Pollefeys, and Davide Scaramuzza. Foresightnav: Learning scene imagination for efficient exploration. In *Proceedings of the Computer Vision and Pattern Recognition Conference*, pages 5236–5245, 2025.
- [38] Vishnu D Sharma, Jingxi Chen, and Pratap Tokekar. Proxmap: Proximal occupancy map prediction for efficient indoor robot navigation. In *2023 IEEE/RSJ International Conference on Intelligent Robots and Systems (IROS)*, pages 7135–7140. IEEE, 2023.
- [39] Chenxu Wang, Xinghang Li, Dunzheng Wang, Huaping Liu, et al. Dynamic scene generation for embodied navigation benchmark. In *RSS 2024 Workshop: Data Generation for Robotics*.
- [40] Hanqing Wang, Wei Liang, Luc Van Gool, and Wenguan Wang. Dreamwalker: Mental planning for continuous vision-language navigation. In *Proceedings of the IEEE/CVF international conference on computer vision*, pages 10873–10883, 2023.
- [41] Yunheng Wang, Yuetong Fang, Taowen Wang, Yixiao Feng, Yawen Tan, Shuning Zhang, Peiran Liu, Yiding Ji, and Renjing Xu. Dreamnav: A trajectory-based imaginative framework for zero-shot vision-and-language navigation. *arXiv preprint arXiv:2509.11197*, 2025.
- [42] Junfeng Wu, Yi Jiang, Qihao Liu, Zehuan Yuan, Xiang Bai, and Song Bai. General object foundation model for images and videos at scale. In *Proceedings of the IEEE/CVF Conference on Computer Vision and Pattern Recognition*, pages 3783–3795, 2024.
- [43] Pengying Wu, Yao Mu, Bingxian Wu, Yi Hou, Ji Ma, Shanghang Zhang, and Chang Liu. Voronav: Voronoi-based zero-shot object navigation with large language model. *arXiv preprint arXiv:2401.02695*, 2024.
- [44] Zhengyuan Yang, Linjie Li, Kevin Lin, Jianfeng Wang, Chung-Ching Lin, Zicheng Liu, and Lijuan Wang. The

- dawn of Imms: Preliminary explorations with gpt-4v (ision). *arXiv preprint arXiv:2309.17421*, 2023.
- [45] Naoki Yokoyama, Sehoon Ha, Dhruv Batra, Jiuguang Wang, and Bernadette Bucher. Vlfm: Vision-language frontier maps for zero-shot semantic navigation. In *2024 IEEE International Conference on Robotics and Automation (ICRA)*, pages 42–48. IEEE, 2024.
- [46] Bangguo Yu, Hamidreza Kasaei, and Ming Cao. L3mvr: Leveraging large language models for visual target navigation. In *2023 IEEE/RSJ International Conference on Intelligent Robots and Systems (IROS)*, pages 3554–3560. IEEE, 2023.
- [47] Lingfeng Zhang, Qiang Zhang, Hao Wang, Erjia Xiao, Zixuan Jiang, Honglei Chen, and Renjing Xu. Trihelper: Zero-shot object navigation with dynamic assistance. In *2024 IEEE/RSJ International Conference on Intelligent Robots and Systems (IROS)*, pages 10035–10042. IEEE, 2024.
- [48] Mingjie Zhang, Yuheng Du, Chengkai Wu, Jinni Zhou, Zhenchao Qi, Jun Ma, and Boyu Zhou. Apexnav: An adaptive exploration strategy for zero-shot object navigation with target-centric semantic fusion. *arXiv preprint arXiv:2504.14478*, 2025.
- [49] Sixian Zhang, Xinyao Yu, Xinhang Song, Xiaohan Wang, and Shuqiang Jiang. Imagine before go: Self-supervised generative map for object goal navigation. In *Proceedings of the IEEE/CVF Conference on Computer Vision and Pattern Recognition*, pages 16414–16425, 2024.
- [50] Qianfan Zhao, Lu Zhang, Bin He, Hong Qiao, and Zhiyong Liu. Zero-shot object goal visual navigation. *arXiv preprint arXiv:2206.07423*, 2022.
- [51] Qianfan Zhao, Lu Zhang, Bin He, and Zhiyong Liu. Semantic policy network for zero-shot object goal visual navigation. *IEEE Robotics and Automation Letters*, 8(11):7655–7662, 2023.
- [52] Kaiwen Zhou, Kaizhi Zheng, Connor Pryor, Yilin Shen, Hongxia Jin, Lise Getoor, and Xin Eric Wang. Esc: Exploration with soft commonsense constraints for zero-shot object navigation. In *International Conference on Machine Learning*, pages 42829–42842. PMLR, 2023.
- [53] Yuke Zhu, Roozbeh Mottaghi, Eric Kolve, Joseph J Lim, Abhinav Gupta, Li Fei-Fei, and Ali Farhadi. Target-driven visual navigation in indoor scenes using deep reinforcement learning. In *2017 IEEE international conference on robotics and automation (ICRA)*, pages 3357–3364. IEEE, 2017.

APPENDIX

We present qualitative examples in both simulated and real-world environments in the attached video. In simulation, we select several challenging cases characterized by severe visual occlusions. For real-world evaluation, we show three indoor scenes: office, classroom, and common room. Please refer to the video for detailed demonstrations.

A. Hyperparameters and System Configuration

In this section, we provide the detailed hyperparameters used in our experiments, including the geometric constraints for trajectory sampling, the coefficients for value map fusion and the FlashWorld Parameters.

1) *Trajectory Sampling Parameters*: The adaptive occluder-aware trajectory sampling strategy is governed by the geometric constraints in Table IV, referencing Eq. 2-6 in Section III.B.1.

TABLE IV: Geometric Constraints and Hyperparameters for Adaptive Trajectory Sampling

| Parameter | Symbol | Value | Description |
|-------------------|----------------|-------|-----------------------------------|
| Ensemble Size | N | 3 | {Left, Right, Up} trajectories |
| Camera Poses | N_{pose} | 24 | Number of views per trajectory |
| Safety Margin | δ | 0.2 m | Buffer added to occluder radius |
| Min Orbital Dist. | d_c^{min} | 1.0 m | Prevents degenerate orbits |
| Angular Expansion | $\Delta\theta$ | 20° | View extension past occluder edge |
| Min Arc Length | d_v^{min} | 1.0 m | Minimum sampling path length |
| Max Arc Length | d_v^{max} | 3.0 m | Maximum sampling path length |

2) *Value Map Fusion Coefficients*: The construction of the Future-Aware Value Map (FAVM) and its fusion with observation cues involves the weights detailed in Table V.

TABLE V: Coefficients for Future-Aware Value Map Construction and Fusion

| Parameter | Symbol | Value | Description |
|----------------------|-----------------|-------|-------------------------------------|
| Fusion Balance | β | 0.5 | Balances real vs. imagination |
| Semantic Weight | α_{sem} | 0.5 | Weight for semantic score $S(g)$ |
| Exploration Weight | α_{exp} | 0.5 | Weight for exploration score $E(g)$ |
| Imagination Discount | λ_{sem} | 0.5 | Discount for hypothesized targets |
| Depth Consistency | τ_d | 0.1 m | Threshold for valid label transfer |

3) *FlashWorld Parameters*: We follow the default parameter settings of FlashWorld, as detailed below:

- Image resolution: 480 × 704;
- Key frames: 24;
- Frame rate: 15 fps.

B. Detailed Definitions of Multi-Sourced Value Maps

In this section, we provide the detailed mathematical definitions and construction procedures for the four components of the observation-based Multi-Sourced Value Map m , defined as $m = m_a + m_s + m_t + m_i$. These maps explicitly model key elements in instruction navigation—actions, landmarks, trajectory history, and intuition—to ground the agent’s decision-making in real-time observations.

1) *Semantic Value Map (m_s)*: The Semantic Value Map encourages the agent to approach landmarks l_{t+1} specified by the high-level planner. We maintain a semantic point cloud \mathcal{P}_{sem} by lifting 2D semantic segmentation masks to 3D using depth observations.

For the current target landmark category, we extract the subset of points $\mathcal{Q} \subset \mathcal{P}_{sem}$. The value for each navigable grid point $p \in \mathcal{G}_{nav}$ is calculated based on its Euclidean distance to the nearest target point:

$$d_{sem}(p) = \min_{q \in \mathcal{Q}} \|p - q\|_2, \quad \forall p \in \mathcal{G}_{nav} \quad (15)$$

To prioritize proximity, we normalize and invert this distance:

$$m_s(p) = 1 - \frac{d_{sem}(p) - \min(d_{sem})}{\max(d_{sem}) - \min(d_{sem})} \quad (16)$$

Thus, regions closer to the observed landmarks receive higher values.

2) *Action Value Map (m_a)*: The Action Value Map translates the discrete action primitive a_{t+1} into a spatial distribution. We initialize m_a with zeros and assign values of 1.0 to specific regions based on the action type:

- **Directional Actions (Move Forward, Turn Left/Right/Around)**: We define a sector corresponding to the intended direction. All navigable points p falling within this sector are assigned $m_a(p) = 1.0$.
- **Explore**: We identify the frontiers (boundaries between free space and unexplored space). Points p near these frontiers are assigned $m_a(p) = 1.0$ to encourage exploration of new areas.
- **Approach**: This action is implicitly handled by the Semantic Value Map (m_s) and does not modify m_a .

3) *Trajectory Value Map (m_t)*: To prevent the agent from revisiting recently traversed areas and getting stuck in loops, the Trajectory Value Map encodes a repulsion field based on the history trajectory $\mathcal{H} = \{h_0, \dots, h_t\}$.

We compute the distance from each grid point p to the nearest history point:

$$d_{traj}(p) = \min_{h \in \mathcal{H}} \|p - h\|_2 \quad (17)$$

Unlike the semantic map, we prefer areas *farther* from the history. The normalized value is given by:

$$m_t(p) = \frac{d_{traj}(p) - \min(d_{traj})}{\max(d_{traj}) - \min(d_{traj})} \quad (18)$$

This assigns higher values to unvisited regions, encouraging diverse navigation trajectories.

4) *Intuition Value Map (m_i)*: The Intuition Value Map (referred to as Heuristic Guidance in the main text) incorporates multimodal reasoning to handle complex instructions or implicit targets not yet explicitly detected.

We employ a Multimodal Large Model (MLM) that takes as input the current panoramic observation O_{pano} , the instruction I , and the current plan. The MLM predicts the most promising

navigation direction D_{pred} . We project the field of view (FOV) corresponding to D_{pred} onto the map:

$$m_i(p) = \begin{cases} 1.0 & \text{if } p \text{ lies within the projected FOV of } D_{pred} \\ 0.0 & \text{otherwise} \end{cases} \quad (19)$$

This component provides heuristic guidance based on common sense even when the target is not visible.

C. Baselines and Implementation Details

In this section, we detail the baseline methods used for comparison, categorized by their underlying navigation paradigms.

1) *Task-Trained Approaches*: The first group of baselines relies on task-specific training, including reinforcement learning or imitation learning on large-scale datasets. This dependence limits their ability to generalize in zero-shot settings.

- **ZSON** [26], **PixNav** [4], **SPNet** [51], and **SGM** [49]: These methods utilize end-to-end training pipelines to learn navigation policies. While effective in trained domains, they often struggle to adapt to unseen environments without fine-tuning.

2) *Zero-Shot Geometric and Semantic Explorers*: The second group consists of methods that perform exploration without task-specific training, leveraging either geometric heuristics or semantic cues.

- **CoW** [12]: Adopts a purely geometric nearest-frontier exploration strategy without explicit semantic reasoning.
- **ESC** [52], **L3MVN** [46], and **TriHelper** [47]: Improve upon pure geometry by first constructing semantic maps. They employ Large Language Models (LLMs) to select promising frontiers based on semantic cues relevant to the target object.
- **VoroNav** [43]: Regularizes exploration by generating frontiers from a Voronoi partition of free space. This approach encourages more structured coverage of the environment.
- **GAMap** [14]: Learns a Gaussian-style value/affordance map to prioritize frontiers that are statistically more likely to contain the target object.

3) *LLM-Based Planning and Advanced Reasoning*: These methods leverage Foundation Models to perform higher-level planning or generate direct guidance signals.

- **VLFM** [45] and **InstructNav** [25]: Go a step further by leveraging LLMs or Vision-Language Models (VLMs) to directly produce value maps. These maps encode preferences over locations and orientations to guide the agent toward the goal.
- **ApexNav** [48] and **CogNav** [5]: Introduce more advanced planning mechanisms. **ApexNav** combines global exploration strategies with local navigation policies to balance coverage and efficiency. **CogNav** maintains a cognitively inspired object-centric map to support long-horizon reasoning and memory.

4) *Implementation of InstructNav**: To ensure a fair comparison with state-of-the-art LLM-driven planners, we implemented a modified version of InstructNav [25], denoted as **InstructNav***.

- **Modifications**: We replaced the original LLM and VLM components with **GPT-4o** to align the reasoning capabilities with our method. Additionally, we utilized **3D Gaussian representations** instead of raw point clouds throughout the pipeline. This modification improves computational efficiency while maintaining the original navigation logic.

D. Qualitative Results

Fig. 7 illustrates the 3DGS scenes generated by the FlashWorld and the simplified 3DGS representation used for planning. The left three columns show the trajectory-conditioned Gaussians imagined from the current observation along three predefined trajectories (left, right, and up). The rightmost column shows the result in simplified representation after downsampling and merging.

E. Failure Case Analysis

While Schrödinger’s Navigator significantly enhances proactive decision-making in occluded environments through trajectory-conditioned imagination and Future-Aware Value Map (FAVM) fusion, we observe several characteristic failure modes. These failures primarily stem from (i) topological and triggering limitations in exploration planning and (ii) cumulative errors in the perception-generation pipeline.

First, in highly occluded and structurally complex scenes, the agent may succumb to local minima or redundant exploration.

- **Sampling Limitations**: Our adaptive trajectory sampling relies on current depth and point cloud clustering. When dealing with non-convex occluders or complex multi-object arrangements, the limited ensemble of candidate trajectories ($N = 3$) may fail to cover the critical “peeking” viewpoint. Consequently, the FAVM may undervalue truly reachable regions in the blind spot, causing the robot to oscillate in narrow areas.
- **Triggering Gaps**: To balance computational efficiency, we employ a periodic or occlusion-driven triggering strategy rather than invoking the world model at every step. This intermittent availability of “future evidence” can lead to myopic decisions during critical moments that require immediate reasoning.

Second, failures also arise from artifacts in the generative process and semantic transfer.

- **Geometric and Scale Drift**: The scale alignment of FlashWorld relies on depth consistency constraints. In regions with weak texture, specular reflections, or high depth noise, these constraints become unreliable, leading to spatial offsets in the imagined free space or candidate targets.
- **High-Confidence Hallucinations**: Semantic labels projected from 2D segmentation to 3DGS can introduce

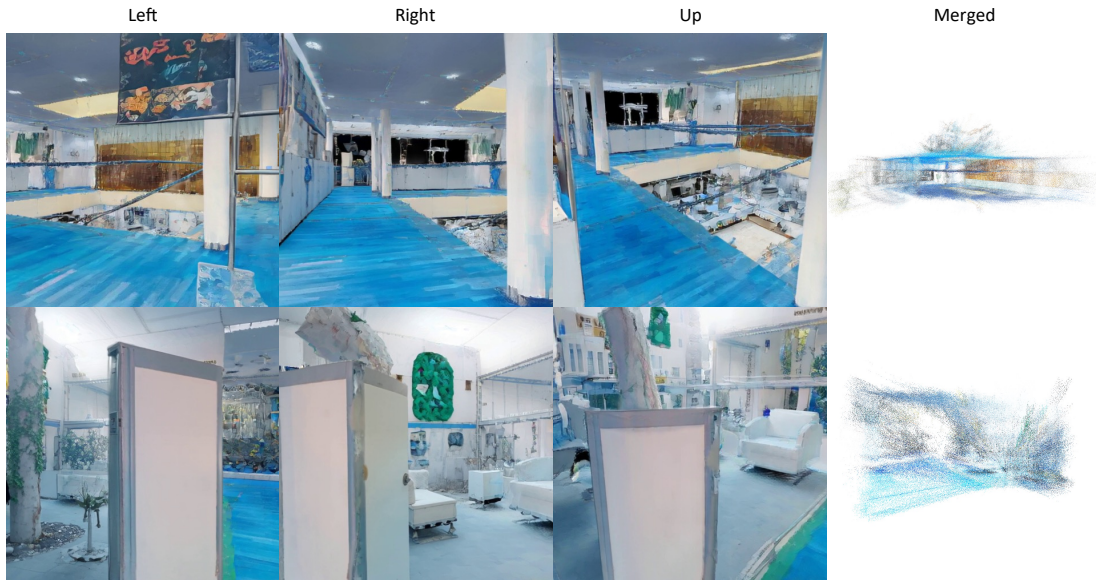


Fig. 7: **Qualitative Simulation Results.** We visualize several navigation examples in the HM3D simulated environments.

errors due to segmentation faults or depth mismatches. These can manifest as “high-confidence hallucinations” of the target. Particularly when the fusion coefficient β heavily favors imagination, the agent may be misled into incorrect regions or stop prematurely due to false positive proximity.

Future work will focus on integrating more robust hierarchical planning to maintain global consistency across regions, alongside uncertainty-aware open-vocabulary perception to mitigate hallucinations. These enhancements aim to translate imaginative insights into actionable navigation gains with greater safety and stability.